

Interfacial DMI in Fe/Pt thin films grown on different buffer layers

Wen-Jun Zhang(张文君), Fei Wei(魏菲), Bing Liu(刘冰), Yang Zhou(周阳), Shi-Shou Kang(康仕寿), and Bing Sun(孙兵)

Citation: Chin. Phys. B, 2024, 33 (**4**): 048501. DOI: 10.1088/1674-1056/ad1b41
Journal homepage: http://cpb.iphy.ac.cn; http://iopscience.iop.org/cpb

What follows is a list of articles you may be interested in

The 50 nm-thick yttrium iron garnet films with perpendicular magnetic anisotropy

Shuyao Chen(陈姝瑶), Yunfei Xie(谢云飞), Yucong Yang(杨玉聪), Dong Gao(高栋), Donghua Liu(刘冬华), Lin Qin(秦林), Wei Yan(严巍), Bi Tan(谭碧), Qiuli Chen(陈秋丽), Tao Gong(龚涛), En Li(李恩), Lei Bi(毕磊), Tao Liu(刘涛), and Longjiang Deng(邓龙江)

Chin. Phys. B, 2022, 31 (**4**): 048503. DOI: 10.1088/1674-1056/ac4cc4

Improved performance of near UV light-emitting diodes with a composition-graded p-AlGaN irregular sawtooth electron-blocking layer

Ping Qin(秦萍), Wei-Dong Song(宋伟东), Wen-Xiao Hu(胡文晓), Yuan-Wen Zhang(张苑文), Chong-Zhen Zhang(张崇臻), Ru-Peng Wang(王汝鹏), Liang-Liang Zhao(赵亮亮), Chao Xia(夏超), Song-Yang Yuan(袁松洋), Yi-an Yin(尹以安), Shu-Ti Li(李述体), Shi-Chen Su(宿世臣)

Chin. Phys. B, 2016, 25 (**8**): 088505. DOI: 10.1088/1674-1056/25/8/088505

Performance improvement of AlGaN-based deep ultraviolet light-emitting diodes with double electron blocking layers

Cheng Zhang(张诚), Hui-Qing Sun(孙慧卿), Xu-Na Li(李旭娜), Hao Sun(孙浩), Xuan-Cong Fan(范宣聪), Zhu-Ding Zhang(张柱定), Zhi-You Guo(郭志友)

Chin. Phys. B, 2016, 25 (**2**): 028501. DOI: 10.1088/1674-1056/25/2/028501

Spin pumping at the $Co_2FeAl_{0.5}Si_{0.5}$/Pt interface

Wu Yong (吴勇), Zhao Yue-Lei (赵月雷), Xiong Qiang (熊强), Xu Xiao-Guang (徐晓光), Sun Young (孙阳), Zhang Shi-Qing (张十庆), Jiang Yong (姜勇)

Chin. Phys. B, 2014, 23 (**1**): 018503. DOI: 10.1088/1674-1056/23/1/018503

Performance improvement of InGaN blue light-emitting diodes with several kinds of electron-blocking layers

Chen Jun(陈峻), Fan Guang-Han(范广涵), Zhang Yun-Yan(张运炎), Pang Wei(庞玮), Zheng Shu-Wen(郑树文), and Yao Guang-Rui(姚光锐)

Chin. Phys. B, 2012, 21 (**5**): 058504. DOI: 10.1088/1674-1056/21/5/058504

Interfacial DMI in Fe/Pt thin films grown on different buffer layers

Wen-Jun Zhang(张文君)[1], Fei Wei(魏菲)[2], Bing Liu(刘冰)[1], Yang Zhou(周阳)[2], Shi-Shou Kang(康仕寿)[2,†], and Bing Sun(孙兵)[1,‡]

[1] *School of Physics and Electronic Information, Weifang University, Weifang* 261061, *China*
[2] *School of Physics and State Key Laboratory of Crystal Materials, Shandong University, Jinan* 250100, *China*

(Received 12 October 2023; revised manuscript received 30 December 2023; accepted manuscript online 5 January 2024)

We study the interfacial Dzyaloshinskii–Moriya interactions (i-DMI) of Fe/Pt bilayers grown on Si substrates with MgO, SiO_2, or Ta each as a buffer layer on the basis of wave-vector-resolved Brillouin light scattering (BLS) measurement. The obtained i-DMI energy values for Fe/Pt on MgO, Ta, and SiO_2 buffer layers are 0.359, 0.321, and 0.274 mJ/m^2, respectively. The large i-DMI value observed in Fe/Pt system on the MgO buffer layer can be attributed to the good interfacial quality and the Rshaba effect at the MgO/Fe interface. Moreover, the MgO/Fe/Pt system, benefiting from better sample quality, exhibits a lower damping factor. Furthermore, layer-resolved first-principles calculations are carried out to gain a more in-depth understanding of the origin of the i-DMI in the Fe/Pt system. The results indicate that in the Fe(110)/Pt(111) system, the substantial DMI energy between Fe spins at the interface is related to a significant change in spin–orbit coupling (SOC) energy in the neighboring Pt layer. In contrast, for the MgO(002)/Fe(002) system, both the DMI and its related SOC energy are concentrated at the interfacial Fe layer. Our investigation will provide a valuable insight into the spintronic community in exploring novel devices with chirality dependence.

Keywords: Fe/Pt, i-DMI, BLS, ferromagnetic resonance, magnetic relaxation

PACS: 75.40.Gb, 85.75.–d **DOI:** 10.1088/1674-1056/ad1b41

1. Introduction

The Dzyaloshinskii–Moriya interaction (DMI),[1,2] which emerges in a system lacking spatial inversion symmetry, has been intensively studied in recent years. The DMI was proposed first by Dzyaloshinskii and Moriya in 1950s to elucidate weak ferromagnetism evidenced in antiferromagnetic crystals,[1] and now it has attracted renewed attention because of its fundamental role in diverse novel phenomena, such as spin spirals,[3,4] cycloids,[4] chiral Néel domain walls (DWs),[5,6] and magnetic skyrmions.[7–14] Especially intriguing are the chiral Néel DWs and magnetic skyrmions because of their great application potentials in new-generation spintronic devices, including racetrack memories[15] and spin logic devices.[16] The DMI can originate from bulk or interfacial properties, depending on the kind of inversion symmetry breaking.[13,17] Notably, the interfacial DMI (i-DMI) generated directly between ferromagnetic (FM) atoms and heavy metal (HM) atoms is predicted to be much stronger and more promising than the bulk one.[18,19] In such a bilayer system, the Hamiltonian representing the DMI between two spins $\boldsymbol{S}_i$ and $\boldsymbol{S}_j$ is expressed as $H_{\mathrm{DMI}} = -\boldsymbol{D} \cdot (\boldsymbol{S}_i \times \boldsymbol{S}_j)$, thus favoring an orthogonal orientation of $\boldsymbol{S}_i$ and $\boldsymbol{S}_j$ with a given chirality depending on the orientation of the i-DMI vector. Consequently, precisely determining the sign and value of $\boldsymbol{D}$ is of utmost importance due to its crucial function in establishing a special chiral spin configuration.

Several experimental methods, such as spin-polarized electron-energy-loss spectroscopy,[20,21] synchrotron-based x-ray scattering,[22] and magneto-optical Kerr-effect microscopy,[23] have been employed to determine the i-DMI energy. Among these methods, Brillouin light scattering (BLS) stands out as the most robust and convenient technique for studying i-DMI in various ferromagnetic/heavy-metal (FM/HM) systems.[24–28] The BLS provides a direct value of the i-DMI energy density through examining the difference in frequency between positive (anti-Stokes) surface spin wave (SW) and negative (Stokes) SW.[25] Several HM/FM systems, such as HM/Co and HM/CoFeB, have been intensively studied in the past few years by using this technique.[24,25,27,29] However, when it comes to the Fe/Pt system, which is theoretically predicted to possess a relatively large i-DMI energy,[30] experimental research is limited.[31] In addition, the use of a suitable buffer layer to enhance interface quality has proved the potential to improve various performance aspects including magnetic properties.[32,33] This approach has found widespread applications in magnetism, particularly in the development of perpendicular magnetic recording media.[33] Nevertheless, the influence of extrinsic properties, such as crystal orientations and interfacial qualities, on i-DMI has rarely been reported.[32]

In this work, we fabricate a series of Fe(3 nm)/Pt(3 nm) bilayers on Si substrates with MgO, SiO_2, or Ta as buffer layers. We conduct BLS and ferromagnetic resonance (FMR) measurements to study the i-DMI and magnetic relaxation in these samples. We find that the i-DMI energy values are 0.274, 0.321, and 0.359 mJ/m^2 for Fe/Pt on SiO_2, Ta, and MgO, re-

†Corresponding author. E-mail: skang@sdu.edu.cn
‡Corresponding author. E-mail: wywdsunbing@wfu.edu.cn

© 2024 Chinese Physical Society and IOP Publishing Ltd

spectively. Furthermore, we confirm that the MgO/Fe interface plays a substantial role in enhancing the i-DMI in the Fe/Pt system fabricated on the MgO buffer layer. Additionally, we thoroughly discuss the influence of crystalline quality and interfacial roughness on the i-DMI strength and Gilbert damping constant. Finally, we use layer-resolved first-principles calculations to further elucidate the origin of the i-DMI energy in the MgO/Fe/Pt system.

2. Experiment details and calculation methods

We used magnetron sputtering at room temperature to fabricate thin films of Fe(3)/Pt(3) (with all thickness values in nanometers). These films were deposited on thermally oxidized silicon substrates with various buffer layers, including MgO, Ta, and SiO_2. Every sample exhibited an in-plane easy axis with negligible perpendicular magnetic anisotropy (PMA). The chamber was maintained at a base pressure lower than 8×10^{-6} Pa, while a working pressure was 0.5 Pa in the deposition process. The crystalline structure was examined by using Rigaku SmartLab XRD equipment. We utilized a MicroMag 2900 alternating gradient magnetometer (AGM) to measure hysteresis curves, from which the saturation magnetizations (M_s) are determined. The strength of i-DMI was measured by using a wave-vector-resolved Brillouin light scattering system as illustrated in Fig. 1(a). In the BLS arrangement, we adopted the setup corresponding to the Damon–Eshbach surface spin wave (SW) mode,[34] which includes applying a magnetic field H aligned with the surface plane (x axis) and sweeping the in-plane wave vector k in the vertical orientation (y axis). As a consequence of the conservation law of momentum between photons and magnons, the strength of the k is related to the incidence angle (θ) of the laser according to $k = (4\pi/\lambda)\sin\theta$. Thus, the wave-vector-resolved BLS spectrum can be obtained by varying the incidence angle of the laser. For investigating the magnetic relaxation, we measured the microwave resonant absorption by using a broad-frequency FMR system. We located the samples directly above the signal line of a GSG co-planar waveguide (CPW) and then applied a sweeping H parallel to the in-plane direction. By varying the microwave frequency, we obtained a series of resonant fields and line widths.

We conducted layer-resolved first-principles calculations by using a Γ-centered Monkhorst–Pack k-point mesh of $4\times16\times1$, which has been validated to ensure reliable convergence of the DMI results.[35] To achieve accurate outcomes, the energy convergence criteria were less than 1.0×10^{-7} eV, and the structures underwent complete relaxation until the forces acting on the atoms were below 0.001 eV/Å. Then, the Kohn–Sham equations were solved in the absence of the spin–orbit coupling (SOC). Finally, incorporating the SOC into the calculations, we obtained the DMI as the difference in total energy when the orientation of the magnetic moments is constrained with opposite chirality spin configurations.

3. Results and discussion

First, we measure BLS to quantify the strength and chirality of i-DMI for each of the three samples on different buffer layers. Figure 1(b) displays the representative BLS spectra for the MgO(3)/Fe(3)/Pt(3) sample with a magnetic field of about 4 kOe (1 Oe = 79.5775 A·m^{-1}). The incident light angle θ is 50°, corresponding to the wave vector $k = 1.809\times10^7$ rad/m. The spectra indicate the presence of both Stokes and anti-Stokes lines. After Lorentzian fitting the curves and applying mirroring operation, the significant difference (Δf) between the anti-Stokes (f_{AS}) and Stokes (f_S) peaks can be obtained directly from the BLS spectra. As is well known, the size of Δf can quantitatively represent the strength of DMI and Δf is given by[25]

$$\Delta f = \frac{2\gamma D}{\pi M_s}k, \tag{1}$$

where γ denotes the gyromagnetic ratio, M_s represents the saturation magnetization, D is a parameter that effectively signifies the intensity of the i-DMI energy. It is essential to emphasize that the chirality of the i-DMI can be identified by examining the sign of $\Delta f = |f_{aS}| - |f_S|$. By experimental conventions, a positive value of DMI corresponds to a right-handed chirality.[26] It is clear that the absolute $|\Delta f|$ in Fig. 1(b) is definitely proportional to the strength of the i-DMI, while the chirality of the i-DMI in MgO/Fe/Pt is obviously right-handed. By varying the intensity of the applied magnetic field, we can derive the field-related behavior of the frequency associated with the anti-Stokes peaks as illustrated in Fig. 1(c). The solid lines depicted in the figure represent the fittings of the dispersion relation for Damon–Eshbach spin waves, as expressed by the following equation:[36]

$$\omega^2_{MSSW} = \omega_H(\omega_H + \omega_M) + \frac{\omega^2_M}{4}(1 - e^{-2kt}), \tag{2}$$

where $\omega_{MSSW} = 2\pi f_{AS}$, $\omega_H = \gamma H$, $\omega_M = 4\pi\gamma M_s$, and t represents the thickness of the Fe layer. From the information presented in Fig. 1(c), the values of γ can be obtained to be 1.917×10^7, 1.915×10^7, and 1.797×10^7 rad/(sOe) for the SiO_2/Fe/Pt, Ta/Fe/Pt, and MgO/Fe/Pt samples, respectively. Then by varying the incident angle between 0° and 80°, i.e. varying k from 0 to 2.32×10^7 rad/m, the dependence of frequency difference on the wave vector can be obtained as shown in Fig. 1(d). By linear fitting using Eq. (1), the i-DMI energy (D) is determined to be 0.274 mJ/m^2, 0.321 mJ/m^2, and 0.359 mJ/m^2 for SiO_2/Fe/Pt, Ta/Fe/Pt, and MgO/Fe/Pt, respectively, and these values are summarized in Table 1. They are slightly smaller than those of the Co/Pt system but much larger than those of the W/CoFeB system or IrMn/CoFeB system.[27,37] It is essential to emphasize here that the energy of i-DMI for the MgO/Fe/Pt system is much stronger than that for the SiO_2/Fe/Pt system and Ta/Fe/Pt system.

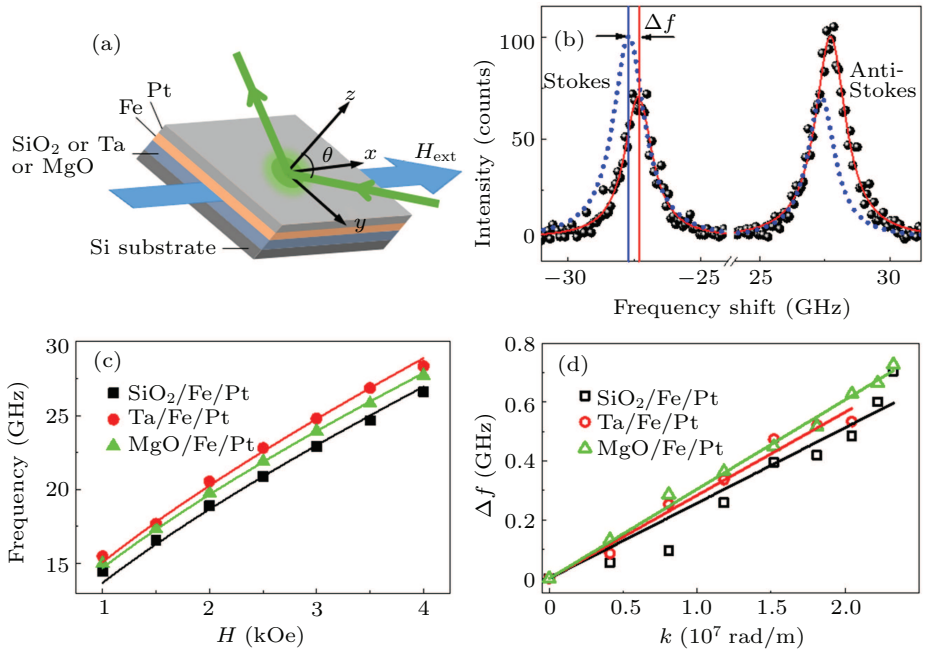


Fig. 1. (a) Schematic diagram of sample structure and geometry for BLS measurement. (b) BLS spectra (solid circles) of MgO/Fe/Pt sample, with experimental conditions involving a wave vector (k) of 1.809×10^7 rad/m and a magnetic field (H) of 4000 Oe (1 Oe = 79.5775 A·m^{-1}), Red curves representing Lorentzian fittings, and blue dashed lines denoting mirrored curves. (c) Relationships between frequency of DE mode and H for the three samples, with solid lines representing fits according to Eq. (2). (d) Relationships between k and Δf for three samples, with solid lines representing linear fits by using Eq. (1).

Since our Fe/Pt system is fabricated on different buffer layers, both interfaces (NM/Fe, Fe/Pt) should have considerable contributions to i-DMI in our nonmagnetic material/ferromagnet/Pt (NM/FM/Pt) trilayer structure.[26] Hence, we should measure the wave-vector-resolved BLS spectra of Al/Fe/SiO_2, Al/Fe/Pt, Al/Fe/Ta, and Al/Fe/MgO structures. Usually, the i-DMI of the Fe/Al interface can be disregarded due to the inherently weak spin–orbit coupling in Al, and the i-DMI should be mainly generated by the other interface. As shown in Figs. 2(a)–2(d), the sign of $\Delta f = |f_{aS}| - |f_S|$ of Fe/Pt is different from the other three samples, suggesting that the chirality of i-DMI in Fe/Pt is opposite to others. Clearly, the i-DMI of Fe/Pt shows right-handed chirality, while the others exhibit left-handed chirality. Moreover, for the Fe/Pt system, the frequency difference Δf demonstrates a maximum, while for the Fe/SiO_2 system, it shows a minimum, suggesting a relatively large energy of i-DMI in the Fe/Pt system. In order to gain more details about the DMI, we conduct a thorough analysis of the Δf with respect to the wave vector k, as displayed in Fig. 2(e). The experimental data evidently exhibit a reasonably linear relationship. By using Eq. (1) and performing a linear fit on Fig. 2(e), we extract the i-DMI energy D, which is summarized in Fig. 2(f) and Table 1. Once again, the i-DMI of Fe/Pt exhibits a right-handed chirality with a relatively large value. The values of i-DMI energy (D) are 0.045 mJ/m^2, 0.092 mJ/m^2, 0.108 mJ/m^2, and 0.258 mJ/m^2 for Fe/SiO_2, Fe/Ta, Fe/MgO, and Fe/Pt, respectively. We should emphasize that the i-DMI in FM/oxide system can be enhanced owing to the presence of Rashba spin–orbit coupling.[38] As is well known, the i-DMI can be notably enhanced when the ferromagnetic (FM) layer is located between two separate NM_1 (NM_2) layers, where the i-DMI exhibits a different chirality for NM_1/FM and NM_2/FM, respectively. Certainly, the measured strength of the i-DMI in an NM/Fe/Pt trilayer is almost equal to the summation of the i-DMI energy observed at the two individual interfaces, namely NM/Fe and Fe/Pt as shown in Figs. 1(d) and 2(e). The i-DMI of the Fe/MgO interface is greater than that of Fe/SiO_2 and Fe/Ta, which preliminarily explains the large i-DMI in the MgO/Fe/Pt trilayer, compared with that in SiO_2/Fe/Pt system and Ta/Fe/Pt system.

It is well known that the i-DMI is strongly dependent on the structure, crystalline quality, and interface roughness. In order to explore the influence of crystalline structure on the observed i-DMI in the Fe/Pt system, we perform XRD measurements on MgO(5)/Fe(10) sample and Ta(5)/Fe(10) sample. In Fig. 3(a), XRD θ–2θ scans for these two samples reveal that Fe exhibits (110) orientation on Ta buffer layer and (002) orientation on MgO buffer layer. The (110) orientation of Fe on the Ta buffer layer is expected because the 5-nm-thick Ta buffer layer is almost amorphous or nano-crystalline when deposited on an amorphous surface, and Fe deposited by sputtering has a (110) preferred orientation on an amorphous surface. It is worth mentioning here that the XRD pattern for Fe/Pt on SiO_2 exhibits a very similar behavior to that on the Ta buffer layer. However, for MgO/Fe, MgO deposited by sputtering has a (002) preferred orientation on an amorphous surface, and then the Fe layer can quasi-epitaxially grow on the MgO buffer layer with (002) orientation. Eventually, the Fe (002) orientation may further enhance the quasi-epitaxial growth of Pt,[39] resulting in good crystalline quality, a smooth interface, and a larger i-DMI of Fe/Pt on MgO.

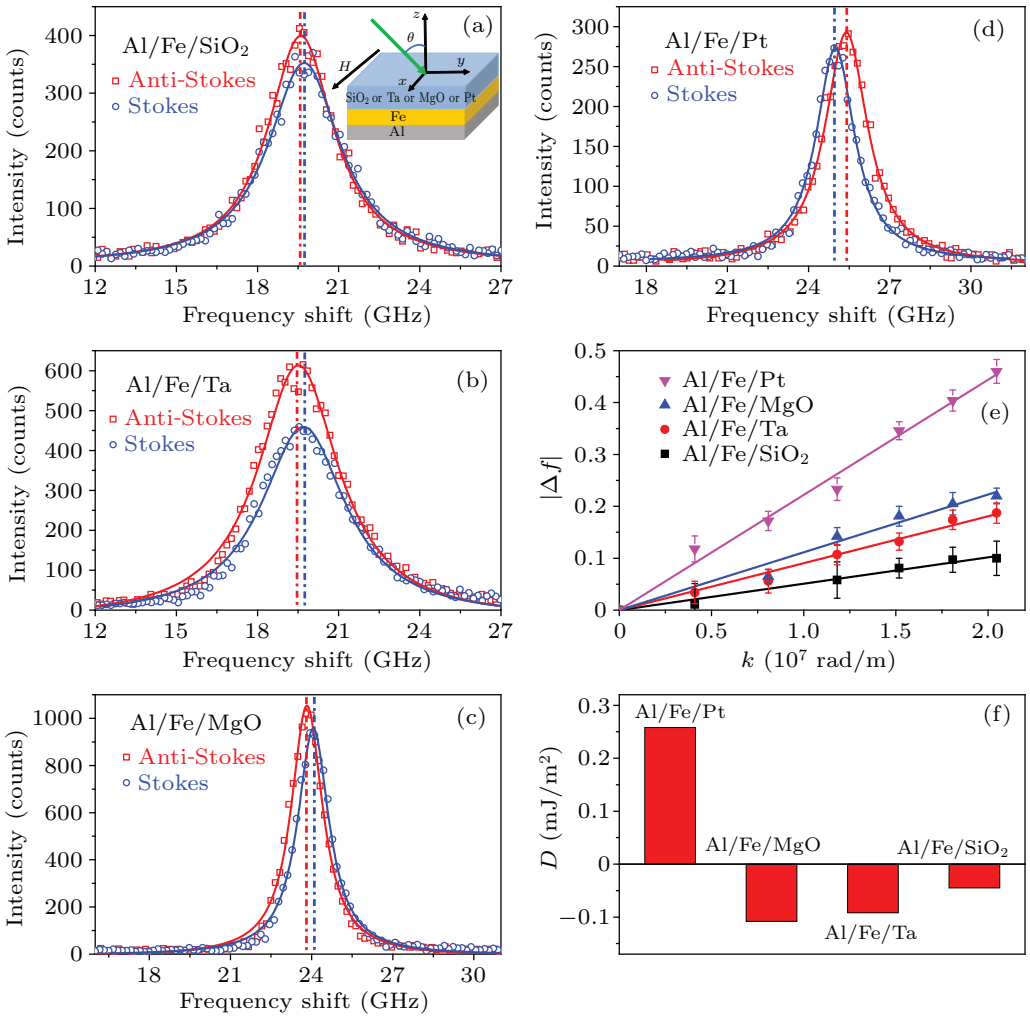


Fig. 2. (a)–(d) BLS spectra (represented by open symbols) obtained from measurements on Al(3)/Fe(3)/SiO_2(3), Al(3)/Fe(3)/Ta(3), Al(3)/Fe(3)/MgO(3), and Al(3)/Fe(3)/Pt(3) at wave vector (k) of 2.046×10^7 rad/m and a magnetic field (H) of 4000 Oe, with solid line showing data fitting Lorentzian curve, Δf representing frequency difference Δ calculated by subtracting frequency of Stokes peak (f_S) from anti-Stokes peak (f_{aS}), and inset in panel (a) illustrating experimental setup. (e) Relationships between the k and the $|\Delta f|$ observed in samples with chiralities, with solid lines representing linear fits by using Eq. (1). (f) Values of i-DMI obtained from Eq. (1) for bilayer structures.

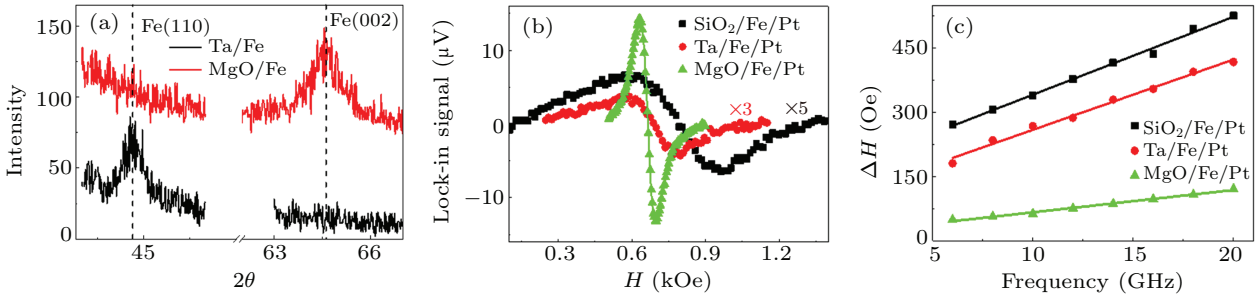


Fig. 3. (a) XRD patterns for Ta/Fe (black line), MgO/Fe (red line), (b) FMR spectra for the three samples were measured at 10 GHz. (c) Variations of the FMR linewidth with frequency for three samples, with solid lines showing linear fits by Eq. (3).

We also perform FMR measurements for these samples to investigate their magnetic relaxation, which might be closely related to the crystalline quality. Figure 3(b) illustrates the typical FMR spectra for these samples, with the signals for Fe/Pt on SiO_2 and Ta magnified by 5 and 3 times, respectively. Obviously, the FMR absorption of Fe/Pt on MgO is much stronger than that on SiO_2 and Ta. Moreover, the linewidth for MgO/Fe/Pt is considerably narrower than those for the other two samples, which further indicates the good crystalline quality of Fe grown on MgO. Figure 3(c) shows the variations of linewidth (ΔH) with frequency for these samples, and all of them exhibit the following linear relation[40]

$$\Delta H = \Delta H_{\text{inh}} + \frac{4\pi\alpha f}{\sqrt{3}\gamma}, \tag{3}$$

where α is Gilbert damping constant, γ is the gyromagnetic ratio, ΔH_{inh} is the inhomogeneous broadening and is related to

film quality. The significant variation in ΔH_{inh} indicates a substantial difference in film quality among these samples. There is no doubt that the epitaxial Fe on the MgO buffer layer has the best quality, while Fe on the SiO_2 buffer layer may exhibit an island growth model. From Fig. 3(c), through fitting with Eq. (3), the Gilbert damping constant α, which characterizes magnetic relaxtion, is extracted. The values of α are 0.044, 0.040, and 0.012 for Fe/Pt samples deposited on SiO_2, Ta, and MgO buffer layers, respectively, and summarized in Table 1. It is important to mention that the α value of MgO/Fe/Pt is extremely lower than those of the other two samples, which may be attributed to the good film quality. The Ta/Fe/Pt and SiO_2/Fe/Pt have very similar α values, although Fe on the Ta buffer layer has better film quality than that on the SiO_2 buffer layer since the ΔH_{inh} is much smaller for Ta/Fe/Pt. However, the presence of an additional spin pumping effect at the Ta/Fe interface may increase the value of α.

In order to further clarify the origin of the i-DMI, we conduct layer-resolved first-principles calculations to determine the theoretical energy of DMI within these structures. Figure 4(a) shows the crystalline structure of Fe(002)/Pt(002), comprising three Fe monolayers, three Pt monolayers, and a 15-Å-thick vacuum layer. By evaluating spin configurations, as illustrated in Figs. 4(a) and 4(b), wherein a single layer exhibits spins with opposite chiralities, while spins in all remaining layers are limited to be aligned along the y axis, we calculated the layer-resolved amplitude of the DMI vector, which is denoted as d^k.[35] The magnitude of d^k is determined from the formula $d^k = (E_{\text{RH}} - E_{\text{LH}})/12$, where E_{RH} and E_{LH} denote the energy associated with right-handed chirality and left-handed chirality, respectively. It is worth noting that the sign convention for DMI in experiment is different from that in calculation. Specifically, in the calculation, a positive DMI represents the left-handed chirality, while in experiment, a negative DMI refers to the left-handed chirality.

Table 1. Magnetic characteristics: asymptotic values of the gyromagnetic ratio (γ), saturation magnetization (M_s), and Gilbert damping constant (α), determined through broadband FMR measurements and using superconducting quantum-interference device.

	γ	M_s	D (mJ/m^2)	α
SiO_2/Fe/Pt	1.917	1136	0.274	0.044
Ta/Fe/Pt	1.915	1334	0.321	0.040
MgO/Fe/Pt	1.797	1418	0.359	0.012
Al/Fe/Pt	1.792	1133	0.258	0.022
Al/Fe/MgO	1.804	1187	0.108	0.015
Al/Fe/Ta	1.802	1112	0.092	0.019
Al/Fe/SiO_2	1.823	1012	0.045	/

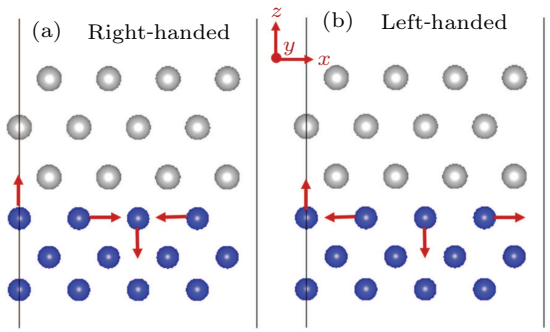


Fig. 4. Examples of (a) right-handed and (b) left-handed spin configuration used for calculating DMI of Fe(002)/Pt(002) bilayers, with blue and silver referring to Fe and Pt, respectively.

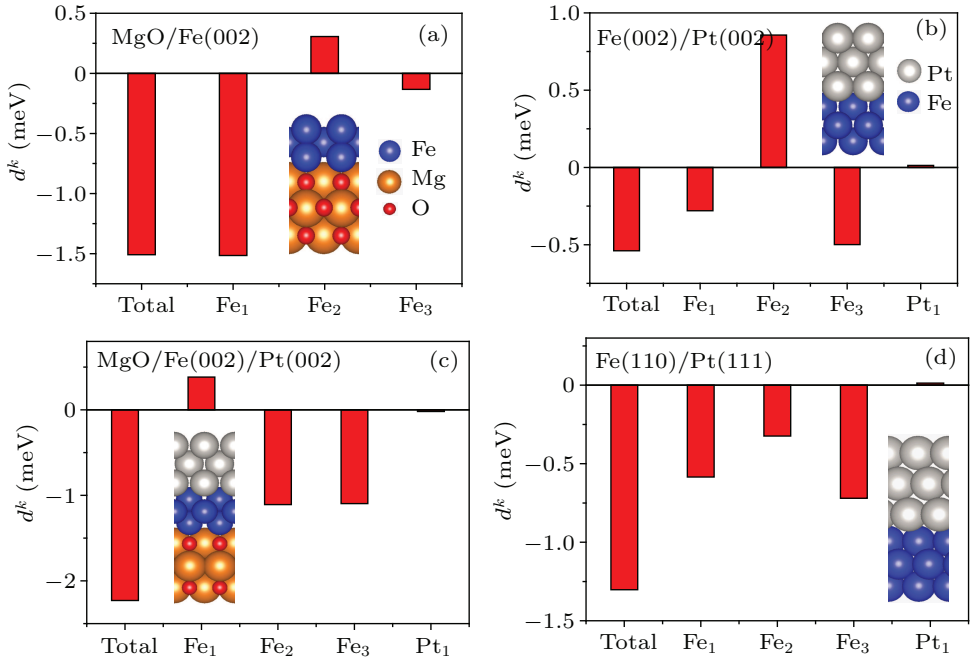


Fig. 5. Layer-resolved DMI coefficient d^{dot} and d^k as a function of layer k for (a) MgO/Fe(002), (b) Fe(002)/Pt(002), (c) MgO/Fe(002)/Pt(002), and (d) Fe(110)/Pt(111) systems.

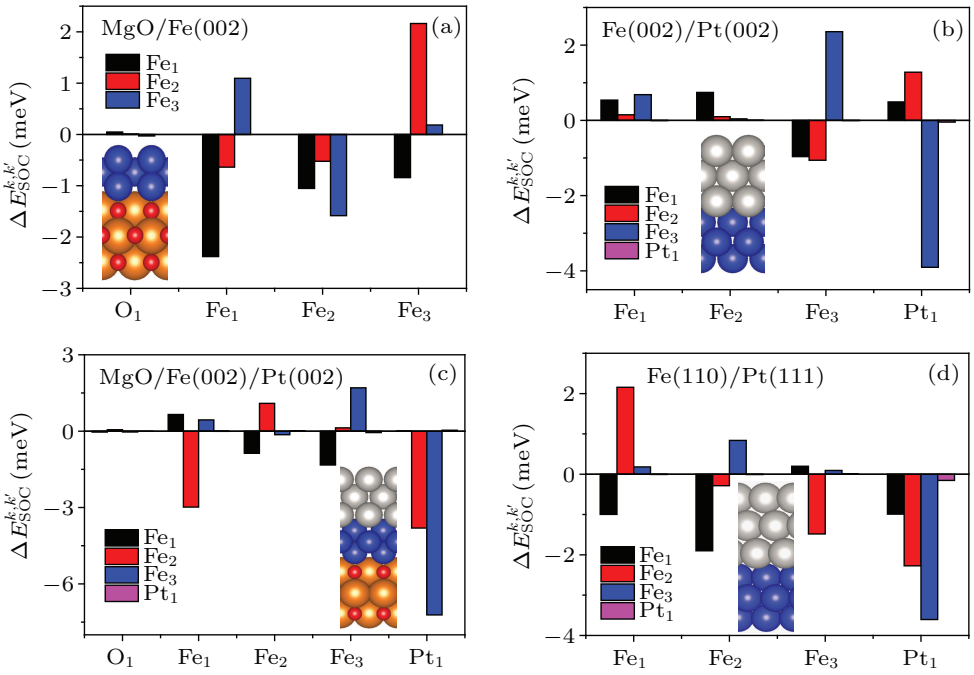


Fig. 6. Spatial distributions of relevant source of SOC energy in atomic sites of different layers k' for (a) MgO/Fe(002) system, (b) Fe(002)/Pt(002) system, (c) MgO/Fe(002)/Pt(002) system, and (d) Fe(110)/Pt(111) system.

Figures 5(a)–5(c) show the outcomes of the layer-resolved DMI vector amplitude $d^{\rm tot}$ and d^k versus layer k for the MgO(002)/Fe(002), Fe(002)/Pt(002), and MgO(002)/Fe(002)/Pt(002) structures, respectively. It is clear that the contribution of the interfacial Fe layer to d^k is considerable. Meanwhile, the resulting total i-DMI strength $d^{\rm tot}$ of MgO/Fe/Pt trilayer is nearly equivalent to the combined contributions of the two separate interfaces (MgO/Fe and Fe/MgO) in this trilayer system. Interestingly, the total i-DMI strength $d^{\rm tot}$ of the MgO/Fe interface is greater than that of the Fe/Pt interface as shown in Figs. 5(a) and 5(b), which further indicates that the i-DMI energy mainly comes from the interface of MgO/Fe in the MgO(002)/Fe(002)/Pt(002) trilayer structure.We also calculate the $d^{\rm tot}$ and d^k of the Fe(110)/Pt(111) structure as shown in Fig. 5(d). It is obvious that the contributions of Fe/Pt interfaces with different crystalline orientations to d^k are quite different. Unfortunately, we cannot calculate the MgO/Fe(110)/Pt(111) system because of the lattice mismatching.

To investigate the spatial origin of each d^k, we calculated $\Delta E_{\rm SOC}^{k,k'}$, which is the difference in SOC energy in layer k',[41] generated by spin setups with different chiralities in layer k. Figures 6(a)–6(d) illustrate the distributions of SOC energy relating to $d^{\rm tot}$ and d^k for all structures. It is the most notable that the distribution of SOC energy is mainly concentrated at the interfacial Pt layer for Fe/Pt structure. For instance, as indicated in Fig. 6(d), the significant DMI energy between the Fe spins at the interface ($k = {\rm Fe_3}$) relates to a substantial SOC energy change $\Delta E_{\rm SOC}^{\rm Fe_3,Pt_1}$ in the neighboring $\rm Pt_1$ layer. Conversely, at the MgO/Fe interface, both the DMI and its related SOC energy are concentrated at the interfacial Fe layer, revealing a distinct mechanism.[38]

4. Conclusions

In this work, we performed the wave-vector-resolved BLS measurements on the Fe/Pt system fabricated on different buffer layers. The i-DMI energy values are determined by fitting the linear relationship between Δf of the anti-Stokes peak and Stokes peak and the wave vector k, resulting in values of 0.274, 0.321, and 0.359 mJ/m^2 for Fe/Pt on SiO_2, Ta, and MgO, respectively. The origin of the large i-DMI in the MgO/Fe/Pt system is verified through two facts. One is that the quasi-epitaxial growth of Fe/Pt on MgO(002) results in a sharp interface, leading to a large i-DMI in this system, and the other is that the strong Rashba effect at the MgO/Fe interface further enhances the i-DMI in this system. In addition, the first-principles calculations revealed that the i-DMI resulting from the contribution of the MgO/Fe interface was taken into consideration in the MgO/Fe/Pt system. These results will be beneficial for the application of chirality-based devices.

Acknowledgements

Project supported by the National Basic Research Program of China (Grant Nos. 12074220, 12304151, 12204355, and 12204356) and the Natural Science Foundation of Shandong Province, China (Grant No. ZR2022QA085).

References

[1] Dzyaloshinsky I 1958 *J. Phys. Chem. Solids* **4** 241

[2] Moriya T 1960 *Phys. Rev. Lett.* **4** 228

[3] Uchida M, Onose Y, Matsui Y and Tokura Y 2006 *Science* **311** 359

[4] Ferriani P, Bergmann K von, Vedmedenko E Y, Heinze S, Bode M, Heide M, Bihlmayer G, Blügel S and Wiesendanger R 2008 *Phys. Rev. Lett.* **101** 027201

[5] Robertson M, Agostino C J, Chen G, Kang S P, Mascaraque A, Michel E G, Won C, Wu Y, Schmid A K and Liu K 2020 *Phys. Rev. B* **102** 024417

[6] Perini M, Meyer S, Dupé B, Malottki S von, Kubetzka A, Bergmann K von, Wiesendanger R and Heinze S 2018 *Phys. Rev. B* **97** 184425

[7] Jiang W, Upadhyaya P, Zhang W, Yu G, Jungfleisch M B, Fradin F Y, Pearson J E, Tserkovnyak Y, Wang K L, Heinonen O, Velthuis S G E te and Hoffmann A 2015 *Science* **349** 283

[8] Zhang Y, Liu J, Dong Y, Wu S, Zhang J, Wang J, Lu J, Rückriegel A, Wang H, Duine R, Yu H, Luo Z, Shen K and Zhang J 2021 *Phys. Rev. Lett.* **127** 117204

[9] Tang J, Wu Y, Wang W, Kong L, Lv B, Wei W, Zang J, Tian M and Du H 2021 *Nat. Nanotechnol.* **16** 1086

[10] Wu Y, Jiang J and Tang J 2022 *Chin. Phys. B* **31** 077504

[11] Tang J, Kong L, Wang W, Du H and Tian M 2019 *Chin. Phys. B* **28** 087503

[12] Liu C, Jiang J, Zhang C, Wang Q, Zhang H, Zheng D, Li Y, Ma Y, Algaidi H, Gao X, Hou Z, Mi W, Liu J, Qiu Z and Zhang X 2023 *Adv. Sci.* **10** 2303443

[13] Yu G, Upadhyaya P, Li X, Li W, Kim S K, Fan Y, Wong K L, Tserkovnyak Y, Amiri P K and Wang K L 2016 *Nano Lett.* **16** 1981

[14] Tang J, Wu Y, Kong L, Wang W, Chen Y, Wang Y, Soh Y, Xiong Y, Tian M and Du H 2021 *National Science Review* **8** nwaa200

[15] Belrhazi H and Hafidi M El 2022 *Sci. Rep.* **12** 15225

[16] Wang W, Sheng Y, Zheng Y, Ji Y and Wang K 2022 *Adv. Electron. Mater.* **8** 2200412

[17] Mühlbauer S, Binz B, Jonietz F, Pfleiderer C, Rosch A, Neubauer A, Georgii R and Böni P 2009 *Science* **323** 915

[18] Seki S, Okamura Y, Kondou K, Shibata K, Kubota M, Takagi R, Kagawa F, Kawasaki M, Tatara G, Otani Y and Tokura Y 2016 *Phys. Rev. B* **93** 235131

[19] Iguchi Y, Uemura S, Ueno K and Onose Y 2015 *Phys. Rev. B* **92** 184419

[20] Zakeri K H, Zhang Y, Prokop J, Chuang T H, Sakr N, Tang W X and Kirschner J 2010 *Phys. Rev. Lett.* **104** 137203

[21] Perini M, Meyer S, Dupé B, Malottki S V, Kubetzka A, Bergmann K V, Wiesendanger R and Heinze S 2018 *Phys. Rev. B* **97** 184425

[22] Dmitrienko V E, Ovchinnikova E N, Collins S P, Nisbet G, Beutier G, Kvashnin Y O, Mazurenko V V, Lichtenstein A I and Katsnelson M I 2014 *Nat. Phys.* **10** 202

[23] Balk A L, Kim K W, Pierce D T, Stiles M D, Unguris J and Stavis S M 2017 *Phys. Rev. Lett.* **119** 077205

[24] Gusev N S, Sadovnikov A V, Nikitov S A, Sapozhnikov M V and Udalov O G 2020 *Phys. Rev. Lett.* **124** 157202

[25] Tacchi S, Troncoso R E, Ahlberg M, Gubbiotti G, Madami M, Åerman J and Landeros P 2017 *Phys. Rev. Lett.* **118** 147201

[26] Zhang W, Jiang B, Wang L, Fan Y, Zhang Y, Yu S Y, Han G B, Liu G L, Feng C, Yu G H, Yan S S and Kang S 2019 *Phys. Rev. Appl.* **12** 064031

[27] Ma X, Yu G, Razavi S A, Sasaki S S, Li X, Hao K, Tolbert S H, Wang K L and Li X 2017 *Phys. Rev. Lett.* **119** 027202

[28] Di K, Zhang V L, Lim H S, Ng S C, Kuok M H, Yu J, Yoon J, Qiu X and Yang H 2015 *Phys. Rev. Lett.* **114** 047201

[29] Srivastava T, Schott M, Juge R, *et al.* 2018 *Nano Lett.* **18** 4871

[30] Kashid V, Schena Timo, Zimmermann B, Mokrousov Y, Blügel S, Shah V and Salunke H G 2014 *Phys. Rev. B* **90** 054412

[31] Zhang W, Chen R, Jiang B, Zhao X, Zhao W, Yan S S, Han G, Yu S, Liu G and Kang S 2021 *Nanoscale* **13** 2665

[32] Kim N H, Han D S, Jung J, Cho J, Kim J S, Swagten H J M and You C Y 2015 *Appl. Phys. Lett.* **107** 142408

[33] Shaw J M, Nembach H T, Silva T J, Russek S E, Geiss R, Jones C, Clark N, Leo T and Smith D J 2009 *Phys. Rev. B* **80** 184419

[34] Damon R W and Eshbach J R 1961 *J. Phys. Chem. Solids* **19** 308

[35] Yang H, Thiaville A, Rohart S, Fert A and Chshiev M 2015 *Phys. Rev. Lett.* **115** 267210

[36] Hillebrands B 1990 *Phys. Rev. B* **41** 530

[37] Chaurasiya A K, Banerjee C, Pan S, Sahoo S, Choudhury S, Sinha J and Barman A 2016 *Sci. Rep.* **6** 32592

[38] Yang H X, Boulle O, Cros V, Fert A and Chshiev M 2018 *Sci. Rep.* **8** 12356

[39] Huo Y, Zeng F L, Zhou C and Wu Y Z 2017 *AIP Adv.* **7** 056024

[40] Oates C J, Ogrin F Y, Lee S L, Riedi P C and Smith G M 2002 *J. Appl. Phys.* **91** 1417

[41] Hallal A, Yang H X, Dieny B and Chshiev M 2013 *Phys. Rev. B* **88** 184423